

LETTER TO THE EDITOR

Discovery of 1*H*-cyclopent[cd]indene (*c*-C₁₁H₈) in TMC-1 with the QUIJOTE line survey: A new three-ringed polycyclic aromatic hydrocarbon[★]

R. Fuentetaja¹, C. Cabezas¹, M. Agúndez¹, B. Tercero^{2,3}, N. Marcelino^{2,3}, P. de Vicente², J. Cernicharo¹

¹ Dept. de Astrofísica Molecular, Instituto de Física Fundamental (IFF-CSIC), C/ Serrano 121, 28006 Madrid, Spain.
e-mail: r.fuentetaja@csic.es, jose.cernicharo@csic.es

² Observatorio de Yebes (IGN), Cerro de la Palera s/n, 19141 Yebes, Guadalajara, Spain.

³ Observatorio Astronómico Nacional (OAN, IGN), C/ Alfonso XIII, 3, 28014, Madrid, Spain.

Received; accepted

ABSTRACT

We report the detection of the polycyclic aromatic hydrocarbon (PAH) 1*H*-cyclopent[cd]indene (*c*-C₁₁H₈) in TMC-1 with the QUIJOTE line survey. We detected 22 independent lines corresponding to 88 rotational transitions with quantum numbers ranging from $J=19$ up to $J=24$ and $K_a \leq 5$ in the Q-band range. The identification of this new PAH was based on the agreement between the rotational parameters derived from the analysis of the lines and those obtained by quantum chemical calculations. The column density derived for 1*H*-cyclopent[cd]indene is $(6.0 \pm 0.5) \times 10^{12} \text{ cm}^{-2}$, with a rotational temperature of 9 K. Its abundance is high, as is that of the rest of the PAHs, but it is the lowest of all those detected to date in TMC-1, being 2.66 times less abundant than indene and 4.66 times less than phenalene. This result will help us to better understand the growth of five- and six-membered rings in dark clouds. Chemical models explaining their formation through the bottom-up model are still very incomplete and require further experimental and theoretical effort. Even so, the most likely formation reactions would occur between the smallest rings with small hydrocarbons; the most probable reaction for the formation of cyclopentindene is that between indene and C₂H, C₂H₃, and/or their cation.

Key words. molecular data — line: identification — ISM: molecules — ISM: individual (TMC-1) — astrochemistry

1. Introduction

The dark cloud TMC-1 has become the best astrophysical source for studying the chemistry of the interstellar medium; it is a natural laboratory where we can evaluate our chemical models. In recent years, more than 70 new molecules have been identified in TMC-1, significantly expanding the known inventory of chemical complexity.

The sensitivity of the Q-band Ultrasensitive Inspection Journey to the Obscure TMC-1 Environment (QUIJOTE) survey has been decisive for these results. It has allowed the detection of species with very low dipole moments (Cernicharo et al. 2021a, 2024a), whose rotational lines have weak intensities, and therefore require long integration times, as in the case of long carbon chains. Among the latest discoveries made with QUIJOTE, we note NC₃S and HC₃S (Cernicharo et al. 2024b); HNC₅ (Fuentetaja et al. 2024); HC₃N⁺, HC₅N⁺, and HC₇N⁺ (Cabezas et al. 2024; Cernicharo et al. 2024c); CH₂CHCHS (Cabezas et al. 2025a); CH₃CHS (Agúndez et al. 2025); and HCCCHCN (Cabezas et al. 2025b).

Among the species detected, polycyclic aromatic hydrocarbons (PAHs) are of particular interest. They are one of the most common types of organic molecules in the interstellar medium and were the first plausible detection using aromatic infrared

bands in the mid-infrared range (Allamandola et al. 1985). However, this technique has not allowed any specific species to be identified. The first unequivocal detection of a PAH occurred in dark clouds and were the cyano-naphthalene derivatives, reported by McGuire et al. (2021), which established an observational precedent for the presence of polycyclic aromatic species in TMC-1. Subsequently, a considerable number of cyano functionalized PAHs were detected in the same cloud, including 2-cyanoindene, cyano-acenaphthylenes, cyano-pyrenes, and cyano-coronene (Sita et al. 2022; Cernicharo et al. 2024a; Wenzel et al. 2024, 2025a,b). The inferred abundances of the corresponding non-functionalized forms were rather high, in the range 10⁻⁹-10⁻⁸ relative to H₂. A clearer picture emerged with the direct detection of a few non-functionalized PAHs, such as indene (Cernicharo et al. 2021a; Burkhardt et al. 2021) and phenalene (Cabezas et al. 2025c). These molecules could be detected in spite of their low dipole moments, well below those of the cyano derivatives observed in TMC-1. The abundances determined for indene and phenalene, above 10⁻⁹ relative to H₂, were consistent with those estimated from the cyano functionalized forms. The observed abundances of PAHs are surprisingly high compared to previous expectations based on extrapolations or analogies with linear species. This forces us to reconsider the role of PAHs in the TMC-1 reaction network (Wakelam & Herbst 2008), both in the gas phase and potentially in interaction with grains, and to improve current chemical models in order to explain their presence in the source. Furthermore, given the existence of such a large PAH as cyanocoronene (with a structure of 24 carbon

[★] Based on observations carried out with the Yebes 40m telescope (projects 19A003, 20A014, 20D023, 21A011, 21D005, and 23A024). The 40m radio telescope at Yebes Observatory is operated by the Spanish Geographic Institute (IGN, Ministerio de Transportes y Movilidad Sostenible).

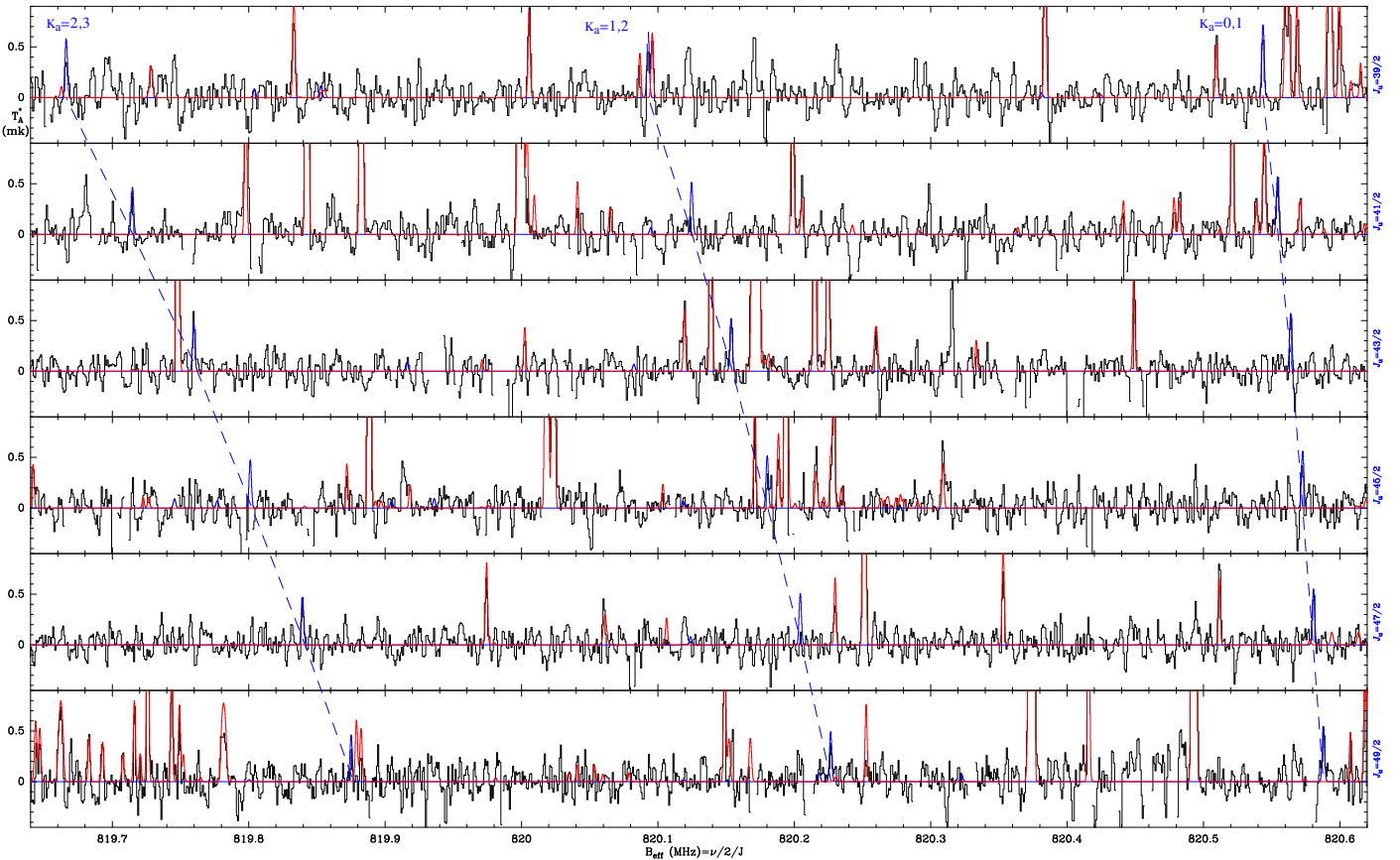


Fig. 1. Modified Loomis–Wood diagram of some of the observed lines of cyclopentindene. The abscissa corresponds to the value of the rotational constant, which has been fixed in this plot to values between 819.6 and 820.6 MHz. The ordinate is the antenna temperature, corrected for atmospheric and telescope losses, in millikelvin. The frequency represented in each box corresponds to $2 B_{\text{rot}} J$, where $J = J_u + 1/2$. The red lines represent a synthetic spectrum of the lines detected with the QUIJOTE data. The blue solid lines correspond to the new detected lines in this work, while dotted lines correspond to transitions with the same K_a (for all transitions involved, see Table B.1).

atoms), we would expect to find a large number of PAHs with comparable sizes having column densities similar to those of the PAHs already detected.

Here we present the detection of 1*H*-cyclopent[cd]indene (hereafter *c*-C₁₁H₈; cyclopentindene), which is the first PAH with two five-atom cycles in its structure and the third unsubstituted PAH detected in the ISM. This discovery will contribute to a better understanding of the formation routes of PAHs containing five- and six-membered rings, which until now have only been studied for cyclopentadiene and indene.

2. Observations

The observational data used belong to QUIJOTE¹ (Cernicharo et al. 2021b, 2024a), a Q-band spectral line survey of TMC-1 performed with the Yebes 40 m telescope at coordinates $\alpha_{J2000} = 4^{\text{h}}41^{\text{m}}41.9^{\text{s}}$ and $\delta_{J2000} = +25^{\circ}41'27.0''$, corresponding to the cyanopolyyne peak (CP) in TMC-1. The receiver was developed within the Nanocosmos project,¹ consisting of two cooled high electron mobility transistor (HEMT) amplifiers covering the 31.0–50.3 GHz band with horizontal and vertical polarization. Fast Fourier transform spectrometers (FFTSs) with 8×2.5 GHz with a spectral resolution of 38.15 kHz provide the whole coverage of the Q-band in both polarizations. A complete description of the system is provided by Tercero et al. (2021). The QUIJOTE survey data presented here were obtained over multiple series of

observation beginning in November 2019. All observations were performed in the frequency-switching observing mode with a frequency throw of either 10 or 8 MHz. The total observing time on source for data taken with frequency throws of 10 MHz and 8 MHz was 772.6 and 736.6 hours, respectively. Hence, the total observing time of the QUIJOTE line survey was 1509.2 hours. Actually, the achieved sensitivity ranged from 0.06 mK at 32 GHz to 0.18 mK at 49.5 GHz, about 100 times better than the earlier Q-band TMC-1 line surveys (Kaifu et al. 2004). A detailed account of the QUIJOTE line survey and the data analysis is given by Cernicharo et al. (2021b, 2022). The main-beam efficiency measured during our 2022 observations varied from 0.66 at 32.4 GHz to 0.50 at 48.4 GHz (Tercero et al. 2021) and across the Q band follows $B_{\text{eff}} = 0.797, \exp[-(\nu/\text{GHz})/71.1]^2$. The forward efficiency of the telescope is 0.97. The half-power beam size is 54.4'' at 32.4 GHz and 36.4'' at 48.4 GHz.

3. Results

Similar to the methodology employed for the detection of other PAHs with the QUIJOTE line survey (Cernicharo et al. 2024a), the analysis began with the identification of a harmonic series from the spectral data, carried out with a modified Loomis–Wood diagram that uses semi-integer $J + 1/2$ values (see Fig. 1). The frequency plotted in each box corresponds to $2C(J + 1/2)$, thus representing the *C* rotational constant on the abscissa axis. These series can be explained by high *J* values,

¹ <https://nanocosmos.iff.csic.es/>

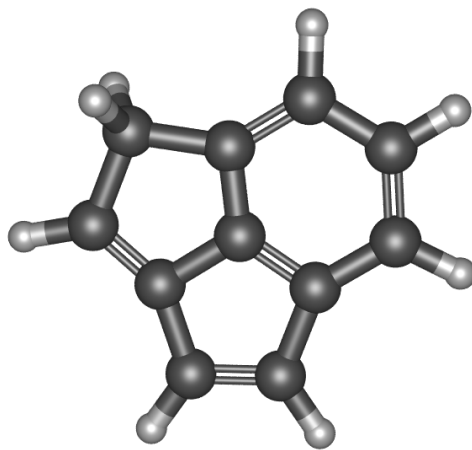


Fig. 2. Optimized geometry of cyclopentindene.

such as those observed in QUIJOTE, using the equations developed by Watson (2007), which provide an equation for the energy in asymptotic cases for asymmetric molecules within the rigid rotor approximation.

We found a new spectral pattern centred around 820.5 MHz, which corresponds to transitions $J=K_c$ (with $K_a=0$ and 1) collapsed at the same frequency (see Table B.1). From there, with the help of the SPFIT programme (Pickett 1991), and using a Watson's Hamiltonian with the A-reduction and the III' representation (Watson 1977), we were able to fit all the observed transitions to higher K_a (see Fig. 1). The derived spectroscopic constants reproduce the observed series with a rms = 6.2 kHz.

Once we have the rotational transitions fitted, we can obtain the molecular constants to identify the molecular carrier responsible of these lines. First of all, the Ray's parameter value ($\kappa = (2B - A - C)/(A - C)$) tells us what type of asymmetric rotor the carrier is. The value obtained for κ is 0.36, which indicates that the molecule is slightly oblate. PAH derivatives, such as the cyano derivatives detected from pyrene, naphthalene, or acenaphthylene, have a prolate structure, so in principle we only consider pure PAHs. Furthermore, the inertia defect ($\Delta_c = I_C - I_B - I_A$) provides the planarity of the molecule. A value of 0 or close to it would mean that the molecule is almost planar. We obtained a value ~ 3.3351 amu \AA^2 , which is very similar to that obtained in the case of phenalene or indene. This indicates that the molecule is mainly planar with two hydrogens outside the plane (Gordy & Cook 1984). Finally, we can use the values of the obtained rotational constants to compare them with other PAHs detected in TMC-1, which indicates the size of the molecule.

Indene has the closest values, but higher than the ones obtained here, which indicates that the new molecule is larger than indene. On the other hand, we see that phenalene has lower values, so we would expect its size to be less than three cycles of six carbon atoms. Within the family of molecules with two six-atom cycles and one five-atom cycle, fluorene does not have a slightly oblate structure; acenaphthylene does not have any hydrogen atoms outside the plane; and both, together with acenaphthene, have constants lower than those obtained. Therefore, the two main candidates we have are 1H-cyclopent[cd]indene and its 2H-cyclopent[cd]indene isomer, which has an energy 94.69129 kJ/mol higher since they are slightly oblate molecules with two

hydrogens outside the plane that have two cycles of five atoms and another cycle of six atoms.

We performed quantum chemical calculations and considered all the information mentioned above. The geometries of the PAHs were optimized using the B3LYP/6-311++G(d,p) level of theory (Becke 1993; Frisch 1984), and the Gaussian 16 package (Frisch 2016), which has been shown to give good results for this type of molecule (Cernicharo et al. 2024a). The results obtained for this molecule, both for the rotational and distortion constants and the dipole moment components, are shown in Table A.1. The values of our search suggest that the best candidate is 1H-cyclopent[cd]indene, whose equilibrium geometry is shown in Fig. 2. The very good agreement between these values and those obtained experimentally confirms that the harmonic series found corresponds to this molecule.

Initially, the observed lines were adjusted taking into account only a-type transitions, but the molecule presents similar values in the μ_a and μ_b components of its dipole moment, 0.6 and 0.8, respectively. Therefore, there is a significant contribution from the b-type transitions that were included in the adjustment. For each detected line, we have four transitions collapsed at the same frequency, two of a-type and two of b-type, with $K_c=J-K_a$ and $K_c=J-K_a-1$.

4. Discussion

Line identification in this work was performed using the MADEX code (Cernicharo 2012). The intensity scale used in this study is the antenna temperature (T_A^*). Consequently, the telescope parameters and source properties were used when modelling the emission of the different species to produce synthetic spectra on this temperature scale. For this work we assumed a velocity for the source relative to the local standard of rest of 5.83 km s^{-1} (Cernicharo et al. 2020). The source was assumed to be circular with a uniform brightness temperature and a radius of $40''$ (Fossé et al. 2001).

To obtain the column density, we assumed that cyclopentindene is close to thermalization ($T_{rot} = 9 \text{ K}$), based on benzonitrile and the other PAHs detected at the source (Cernicharo et al. 2023, 2024a). We derived a column density of $(6.0 \pm 0.5) \times 10^{12} \text{ cm}^{-2}$ (see Fig. 3). This value is the lowest detected in pure PAH in TMC-1. The abundance of cyclopentindene is 2.66 and 4.66 times lower than those of indene and phenalene, respectively. These values were obtained at a T_{rot} of 10 K for indene and $7.9 \pm 1.2 \text{ K}$ for phenalene (Cernicharo et al. 2021a; Cabezas et al. 2025c).

The processes involved in the formation of PAHs are unclear. Chemical models are being improved to try to explain the observed abundance. There are two main hypotheses regarding their formation. The first is the bottom-up model, which proposes that PAHs form in cold dark clouds from smaller hydrocarbons. These molecules would grow and form increasingly larger cycles. The second hypothesis is the top-down model, which considers that small PAHs originate from the fragmentation of very large PAHs coming from outside the cloud. In TMC-1, observational data favour the bottom-up model. Spatial distributions, for example that of benzonitrile, coincide with those of cyanopolyyynes and other reactive species, and therefore the data point to local formation from carbon chains, radicals, and cations detected at the source (Cernicharo et al. 2023).

The chemical pathways involved combine neutral-neutral and ion-neutral reactions. For the formation of single-cycle molecules, the reaction $1\text{-C}_3\text{H}_3^+ + \text{C}_2\text{H}_4 \rightarrow \text{C}_5\text{H}_7^+$ has been shown to be rapid and to reproduce the abundance of cyclopentadiene,

supporting the idea that both types of processes contribute to the growth of PAHs in cold clouds (Cernicharo et al. 2024a).

For three-ringed species, specific bottom-up routes have been proposed. Kaiser & Hansen (2021) proposed the addition of five-carbon cycles through the reaction of vinyl derivatives of PAHs with CH. In acenaphthylene, direct reactions of C₂H or H₂CCH (not detected yet) with naphthalene or C₃H with indene are suggested as potential formers, but further studies are needed to assess the viability of these routes (Cernicharo et al. 2024a). In the case of the pure PAH phenalene, a viable ion neutral pathway has been identified based on radiative association C₁₂H₈ + CH₃⁺ → C₁₃H₁₁⁺ + hν, followed by dissociative recombination to yield C₁₃H₁₀. This pathway is evaluated as exothermic and without a barrier in the association step, highlighting the possible expanded role of ion-molecule chemistry in PAH formation (Cernicharo et al. 2022; Cabezas et al. 2025c). This latter neutral ion pathway has been proposed for all cyclic species with five and six atoms and for the PAHs detected so far in TMC-1 (Loru et al. 2023; Cernicharo et al. 2021a,c,d, 2022, 2024a). Analogous to these PAHs, the reaction of C₂H (or its cation) with indene could be a viable formation pathway for cyclopentindene. Despite all this information, theoretical or experimental processes are still needed to study the possible formation pathways in order to correctly describe their presence.

5. Conclusions

In this work we reported the first detection in the ISM of cyclopentindene, a new three-ringed molecule, based on the visual search of a harmonic pattern and quantum chemistry calculations. The column density derived is $6 \times 10^{12} \text{ cm}^{-2}$. Its abundance is the lowest of all pure PAHs detected in TMC-1 when compared to indene and phenalene. Possible formation pathways for PAHs were discussed, but the chemical models are currently incomplete and further experimental and theoretical studies are needed to properly understand the formation processes and abundances of these species. Finally, the detection of cyanocoronene suggests that in the future we may be able to detect more intermediate-sized PAHs that will aid our understanding of the role these molecules play in the chemistry of the ISM.

Acknowledgements. The present study was supported by Ministerio de Ciencia e Innovación of Spain (MICIU) for funding support through projects PID2023-147545NB-I00 and PID2022-137980NB-100. Also thank ERC for funding through grant ERC-2013-SyG-610256- 312 NANOCOSMOS.

References

Agúndez, M., Molpeceres, G., Cabezas, C., et al. 2025, A&A, 693, L20.
 Allamandola L. J., Tielens, A. G. G. M., Barker J. R., 1985, ApJ 290, L25
 Becke, A. D. 1993, J. Chem. Phys., 98, 2, 1372.
 Burkhardt, A. M., Long Kelvin Lee, K., Bryan Changala, P., et al. 2021, ApJ, 913, L18.
 Cabezas, C., Agúndez, M., Endo, Y., et al. 2024, A&A, 687, L22.
 Cabezas, C., Vávra, K., Molpeceres, G., et al. 2025a, A&A, 698, L24.
 Cabezas, C., Agúndez, M., Marcelino, N., et al. 2025b, A&A, 693, L14.
 Cabezas, C., Agúndez, M., Pérez, C., et al. 2025c, A&A, 701, L8.
 Cernicharo, J., 2012, in ECLA 2011: Proc. of the European Conference on Laboratory Astrophysics, EAS Publications Series, 2012, Ed.: C. Stehl, C. Joblin, & L. d'Hendecourt (Cambridge: Cambridge Univ. Press), 251; https://nanocosmos.iff.csic.es/?page_id=1619
 Cernicharo, J., Marcelino, N., Agúndez, M., et al. 2020, A&A, 642, L8
 Cernicharo, J., Agúndez, M., Cabezas, C., et al. 2021a, A&A, 649, L15.
 Cernicharo, J., Agúndez, M., Kaiser, R. I., et al. 2021b, A&A, 652, L9
 Cernicharo, J., Agúndez, M., Kaiser, R. I., et al. 2021c, A&A, 655, L1
 Cernicharo, J., Agúndez, M., Kaiser, R. I., et al. 2021d, A&A, 652, L9
 Cernicharo, J., Fuentetaja, R., Agúndez, M., et al. 2022, A&A, 663, L9
 Cernicharo, J., Tercero, B., Marcelino, N., et al. 2023, A&A, 674, L4.
 Cernicharo, J., Cabezas, C., Fuentetaja, R., et al. 2024a, A&A, 690, L13
 Cernicharo, J., Cabezas, C., Agúndez, M., et al. 2024b, A&A, 688, L13
 Cernicharo, J., Cabezas, C., Agúndez, M., et al. 2024c, A&A, 686, L15
 Fossé, D., Cernicharo, J., Gerin, M., Cox, P. 2001, ApJ, 552, 168
 Frisch M. J., Pople, J. A., Binkley, J. S. 1984, J. Chem. Phys., 80, 3265
 Frisch M.J., et al. 2016, Gaussian 16 Revision A.03
 Fuentetaja, R., Cabezas, C., Endo, Y., et al. 2024, A&A, 688, L29
 Gordy W., Cook R. 1984, Microwave Molecular Spectra, Techniques of Chemistry (New York: Wiley)
 Kaifu, N., Ohishi, M., Kawaguchi, K., et al. 2004, PASJ, 56, 6
 Kaiser, R. I. & Hansen, N. 2021, Journal of Physical Chemistry A, 125, 3826.
 Loru, D., Cabezas, C., Cernicharo, J., et al. 2023, A&A, 677, A166
 McGuire, B. A., Loomis, R. A., Burkhardt, A. M., et al. 2021, Science, 371, 1265
 Pickett, H. M. 1991, J. Mol. Spectrosc., 148, 371
 Sita, M. L., Changala, P. B., Xue, C., et al. 2022, ApJ, 938, 2, L12.
 Tercero, F., López-Pérez, J. A., Gallego, J. D., et al. 2021, A&A, 645, A37
 Wakelam, V. & Herbst, E. 2008, ApJ, 680, 371
 Watson, J. K. G., in "Vibration Spectra and Structure" (J. Durig, Ed.), Vol.6, p.1, Elsevier, Amsterdam, 1977
 Watson, J. K. G. 2007, Molecular Physics, 105, 5-7, 679. doi:10.1080/00268970701241672
 Wenzel, G., Cooke, I. R., Changala, P. B., et al. 2024, Science, 386, 810.
 Wenzel, G., Speak, T. H., Changala, P. B., et al. 2025, Nature Astronomy, 9, 262.
 Wenzel, G., Gong, S., Xue, C., et al. 2025, ApJ, 984, L36.

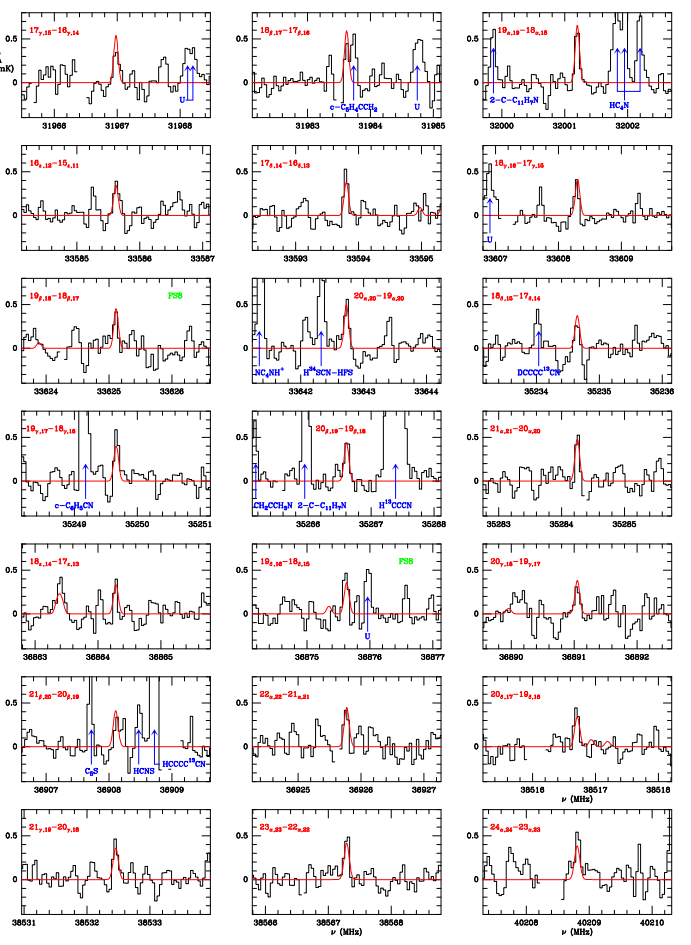


Fig. 3. Some of the cyclopentindene lines observed in TMC-1 with QUIJOTE. The black line represents the survey data, while the red line represents the synthetic spectrum calculated for a column density of $6 \times 10^{12} \text{ cm}^{-2}$. The green labels indicate the transitions for which only the 8 MHz frequency-switching data were used. The blanked channels correspond to negative features resulting in the folding of the frequency-switched spectra. Each box shows four collapsed transitions corresponding to each line, where $\alpha, \beta, \gamma, \delta$, and ϵ are $K_a=0,1$, $K_a=1,2$, $K_a=2,3$, $K_a=3,4$, and $K_a=4,5$, respectively (see Table B.1 for more details about transitions). The unidentified lines or other molecules already detected in the source appear in blue. The abscissa corresponds to the rest frequency assuming a local standard of rest velocity of 5.83 km s^{-1} . The ordinate is the antenna temperature in millikelvin.

Appendix A: Rotational constants

Table A.1. Experimental and theoretical molecular constants of cyclopentindene.

Parameter	1H-cyclopent[cd]indene ^a	2H-cyclopent[cd]indene ^a	TMC-1 (<i>III</i>)
<i>A</i> /MHz	1809.3791	1769.6150	1804.613(71) ^b
<i>B</i> /MHz	1490.4924	1510.4163	1490.725(56)
<i>C</i> /MHz	821.38945	818.97200	820.77500(68)
Δ_J /Hz	45.05	46.95	51.0(45)
Δ_{JK} /Hz	-59.98	-66.53	-66.5(50)
Δ_K /Hz	19.75	24.42	[19.75] ^c
δ_J /Hz	-3.72	-4.73	[-3.72]
δ_K /Hz	24.74	20.26	[24.74]
N_{trans}^d, N_{lines}^e			88, 22
$J_{max}, K_{a,max}$			24, 6
$\sigma(kHz)^f, \sigma_w^g$			6.2, 0.65
μ_a, μ_b	0.60, 0.80	0.28, 1.12	

Notes.

- (*a*) B3LYP/6-311++G(d,p) level of theory.
- (*b*) The uncertainties (in parentheses) are in units of the last significant digits.
- (*c*) Values in square brackets have been kept fixed to the theoretical values.
- (*d*) Total number of rotational transitions.
- (*e*) Total number of independent frequencies.
- (*f*) Standard root mean square deviation of the fit in kHz.
- (*g*) Weighted root mean square deviation of the fit, unitless.

Appendix B: Derived line parameters

The line parameters derived for this work were obtained by fitting a Gaussian line profile to the observed data, using the software Class (GILDAS package). We used a window of ± 15 km s $^{-1}$ around the V_{LSR} (5.83 km s $^{-1}$) of the source for each transition. Negative features in the folding of the frequency switching data were blanked before baseline removal. Several of these transitions can be observed in Fig. 3.

Table B.1. Observed line parameters for cyclopentindene.

Transition	ν_{obs}^a MHz	$\nu_{obs-calc}^l$ MHz	$\int T_A^* dv^b$ mK km s $^{-1}$	Δv^c km s $^{-1}$	$T_A^* d$ mK
17 _{2,15} -16 _{2,14}	31966.982 \pm 0.010	0.004	0.29 \pm 0.09	0.85 \pm 0.27	0.32 \pm 0.10
17 _{3,15} -16 _{2,14}					
17 _{2,15} -16 _{3,14}					
17 _{3,15} -16 _{3,14}					
18 _{1,17} -17 _{1,16}	31983.619 \pm 0.012	0.001	0.28 \pm 0.09	0.55 \pm 0.21	0.47 \pm 0.10
18 _{2,17} -17 _{1,16}					
18 _{1,17} -17 _{2,16}					
18 _{2,17} -17 _{2,16}					
19 _{0,19} -18 _{0,18}	32001.202 \pm 0.010	<0.001	0.52 \pm 0.07	0.73 \pm 0.12	0.68 \pm 0.10
19 _{1,19} -18 _{0,18}					
19 _{0,19} -18 _{1,18}					
19 _{1,19} -18 _{1,18}					
16 _{4,12} -15 _{4,11}	33585.632 \pm 0.010	0.003	0.33 \pm 0.06	0.87 \pm 0.17	0.36 \pm 0.08
16 _{5,12} -15 _{4,11}					
16 _{4,12} -15 _{5,11}					
16 _{5,12} -15 _{5,11}					
17 _{3,14} -16 _{3,13}	33593.799 \pm 0.010	0.003	0.39 \pm 0.08	0.64 \pm 0.13	0.57 \pm 0.10
17 _{4,14} -16 _{3,13}					
17 _{3,14} -16 _{4,13}					
17 _{4,14} -16 _{4,13}					
18 _{2,16} -17 _{2,15}	33608.290 \pm 0.010	0.011	0.36 \pm 0.07	0.74 \pm 0.16	0.45 \pm 0.08
18 _{3,16} -17 _{2,15}					
18 _{2,16} -17 _{3,15}					
18 _{3,16} -17 _{3,15}					
19 _{1,18} -18 _{1,17} ^e	33625.111 \pm 0.010	0.002	0.32 \pm 0.08	0.72 \pm 0.25	0.41 \pm 0.12
19 _{2,18} -18 _{1,17}					
19 _{1,18} -18 _{2,17}					
19 _{2,18} -18 _{2,17}					
20 _{0,20} -19 _{0,19}	33642.731 \pm 0.010	0.003	0.41 \pm 0.09	0.73 \pm 0.19	0.53 \pm 0.10

Table B.1. continued.

Transition	ν_{obs}^a MHz	$\nu_{obs-calc}^l$ MHz	$\int T_A^* dv^b$ mK km s ⁻¹	Δv^c km s ⁻¹	$T_A^* d$ mK
20 _{1,20} -19 _{0,19}					
20 _{0,20} -19 _{1,19}					
20 _{1,20} -19 _{1,19}					
18 _{3,15} -17 _{3,14}	35234.645±0.010	0.001	0.20±0.06	0.61±0.20	0.30±0.09
18 _{4,15} -17 _{3,14}					
18 _{3,15} -17 _{4,14}					
18 _{4,15} -17 _{4,14}					
19 _{2,17} -18 _{2,16}	35249.661±0.010	0.010	0.41±0.06	0.63±0.10	0.60±0.10
19 _{3,17} -18 _{2,16}					
19 _{2,17} -18 _{3,16}					
19 _{3,17} -18 _{3,16}					
20 _{1,19} -19 _{1,18}	35266.615±0.010	0.006	0.40±0.08	0.76±0.18	0.49±0.09
20 _{2,19} -19 _{1,18}					
20 _{1,19} -19 _{2,18}					
20 _{2,19} -19 _{2,18}					
21 _{0,21} -20 _{0,20}	35284.252±0.010	<0.001	0.33±0.05	0.50±0.10	0.62±0.09
21 _{1,21} -20 _{0,20}					
21 _{0,21} -20 _{1,20}					
21 _{1,21} -20 _{1,20}					
17 _{5,12} -16 _{5,11}	36863.401±0.012	0.006	0.48±0.11	1.12±0.32	0.40±0.10
17 _{6,12} -16 _{5,11}					
17 _{5,12} -16 _{6,11}					
17 _{6,12} -16 _{6,11}					
18 _{4,14} -17 _{4,13}	36864.275±0.010	0.004	0.21±0.04	0.33±0.25	0.59±0.10
18 _{5,14} -17 _{4,13}					
18 _{4,14} -17 _{5,13}					
18 _{5,14} -17 _{5,13}					
19 _{3,16} -18 _{3,15} ^e	36875.615±0.010	0.008	0.39±0.08	0.69±0.14	0.53±0.10
19 _{4,16} -18 _{3,15}					
19 _{3,16} -18 _{4,15}					
19 _{4,16} -18 _{4,15}					
22 _{0,22} -21 _{0,21}	36925.765±0.010	0.009	0.27±0.08	0.60±0.14	0.43±0.11
22 _{1,22} -21 _{0,21}					
22 _{0,22} -21 _{1,21}					
22 _{1,22} -21 _{1,21}					
19 _{4,15} -18 _{4,14}	38504.336±0.017	0.009	0.50±0.13	1.02±0.30	0.46±0.12
19 _{5,15} -18 _{4,14}					
19 _{4,15} -18 _{5,14}					
19 _{5,15} -18 _{5,14}					
20 _{3,17} -19 _{3,16}	38516.697±0.010	0.005	0.32±0.07	0.65±0.16	0.47±0.08
20 _{4,17} -19 _{3,16}					
20 _{3,17} -19 _{4,16}					
20 _{4,17} -19 _{4,16}					
21 _{2,19} -20 _{2,18}	38532.453±0.010	0.001	0.28±0.05	0.59±0.11	0.46±0.08
21 _{3,19} -20 _{2,18}					
21 _{2,19} -20 _{3,18}					
21 _{3,19} -20 _{3,18}					
23 _{0,23} -22 _{0,22}	38567.293±0.010	0.002	0.36±0.07	0.64±0.13	0.52±0.09
23 _{1,23} -22 _{0,22}					
23 _{0,23} -22 _{1,22}					
23 _{1,23} -22 _{1,22}					
23 _{1,22} -22 _{1,21}	40191.115±0.012	0.009	0.20±0.05	0.56±0.19	0.33±0.09
23 _{2,22} -22 _{1,21}					
23 _{1,22} -22 _{2,21}					
23 _{2,22} -22 _{2,21}					
24 _{0,24} -23 _{0,23}	40208.816±0.023	0.004	0.30±0.19	0.56±0.45	0.51±0.14
24 _{1,24} -23 _{0,23}					
24 _{0,24} -23 _{1,23}					
24 _{1,24} -23 _{1,23}					

Notes.

(a) Adopted rest frequency (see text).
 (b) Integrated line intensity in mK km s⁻¹.
 (c) Line width at half intensity derived by fitting a Gaussian function to the observed line profile (in km s⁻¹).
 (d) Antenna temperature in millikelvin.
 (e) We obtained the line parameters using only the 8 MHz frequency switching data.